npj | natural hazards

Brief communication

https://doi.org/10.1038/s44304-026-00167-x

Atmospheric rivers are associated with nine out of every 10 floods in major global river basins

Milica Stojanovic[1] ✉, Albenis Pérez-Alarcón[1,2], Rogert Sorí[1], Raquel Nieto[1,3] & Luis Gimeno[1,3]

The role of atmospheric rivers (ARs) in 119 major flood events across 50 global river basins was investigated. The ARs were linked to 74% of the flood areas and 89% of the full basins. Their contributions were evident during and before floods, with influences spanning mid-latitudes to tropical regions, causing human fatalities and population displacements. These findings underscore ARs as dominant and widespread drivers of extreme flood events worldwide.

Atmospheric rivers (ARs) are narrow corridors of intense water vapour moving poleward in the lower troposphere[1,2] typically associated with a low-level jet stream ahead of the cold front of an extratropical cyclone[3]. However, they can also be linked to other meteorological configurations, including low-level jets, tropical plumes, and related large-scale circulation features involving tropical, extratropical, and tropical-extratropical interactions[4,5].

These phenomena frequently drive extreme precipitation and winds over short periods[6], which often result in natural disasters[7], overwhelming river systems and triggering widespread flooding[8]. While ARs contribute 22–50% of total runoff in global river basins and can increase flood occurrence by up to 80% in AR-affected regions[9], their hydrological influence extends beyond these well-documented direct impacts, including drought busters[10]. The role of ARs in preconditioning catchments through antecedent precipitation and their spatial influence beyond flood zones remains poorly quantified.

Floods are among the most frequent and devastating natural disasters worldwide and are responsible for the greatest number of fatalities among all natural hazards, as well as long-term displacement, infrastructure damage, and economic disruption that affect vulnerable populations worldwide[7,11]. As climate change intensifies the hydrological cycle[12], floods have increased substantially across diverse geographic regions[13,14], representing an increasing threat that demands improved understanding of the atmospheric drivers responsible for extreme precipitation and flood generation.

Atmospheric rivers have emerged as a critical driver of flood events globally, yet their role in flood generation across diverse climatic regions remains incompletely characterised. Conventional analyses of ARs have focused largely on their structure, the associated precipitation and impacts along the western coastal areas in midlatitude continents, particularly North America and Europe[15,16]. Nevertheless, their global significance remains incompletely described, as flood generation mechanisms vary across latitudes and continents, with tropical and subtropical basins home to billions remaining understudied. This study focuses on global river basins as they represent fundamental hydrological units that capture the integrated response to atmospheric inputs like precipitation associated with ARs.

To quantify the global relationship between ARs and flooding, the spatiotemporal coincidence of ARs with flood events was analysed. We examined entire river basins, HydroBASINS level 4 and 5 sub-basins[17], representing successive, hierarchically nested subdivisions of the major basins, and flood-affected areas to capture direct impacts and upstream influences, respectively. In addition, analysed ARs activity during flood periods and up to 3 days before, to assess both immediate triggers and antecedent conditioning effects. Using the Global Active Archive of Large Flood Events[18], we identified 119 major flood events across 24 of 50 global river basins between 1999 and 2018 (Fig. 1), with the spatial intersections between flood extents and the corresponding HydroBASINS level 4 and 5 sub-basins shown in Fig. S2. Our analysis reveals striking patterns; 88 of the 119 flood events (74%) were influenced by ARs that directly intersected the inundated region, spanning 18 distinct basins across multiple continents, including the Amazon, Niger, Congo, and Yangtze River basins, where AR impacts on flooding have been largely unquantified (Table S1). When the impact of the AR outside the flood area but within the basin was also considered, this influence expanded to 106 events (89%) across 22 basins, also demonstrating the widespread role of ARs in flood generation beyond direct precipitation zones. The analysis and results, however, are conditional on major floods as documented by the Dartmouth Flood Observatory (DFO). Regions experiencing frequent AR landfalls, such as the U.S. West Coast and Western Europe, do not exhibit strong AR-flood associations in our study, as basin-scale floods meeting DFO criteria were relatively rare during the study period. Furthermore, while our methodology was necessary for consistent global AR-flood attribution analysis within defined hydrological units, it may underrepresent the flood burden in regions with frequent, extensive, transboundary, or seasonally recurring flooding (e.g.

[1]Centro de Investigación Mariña, Environmental Physics Laboratory (EPhysLab), Universidade de Vigo, Ourense, Spain. [2]Instituto Dom Luiz (IDL), Faculdade de Ciências, Universidade de Lisboa, Lisboa, Portugal. [3]Climate System Research Unit, UVigo-CESGA, Santiago de Compostela, Spain.
✉e-mail: mstojanovic@uvigo.es

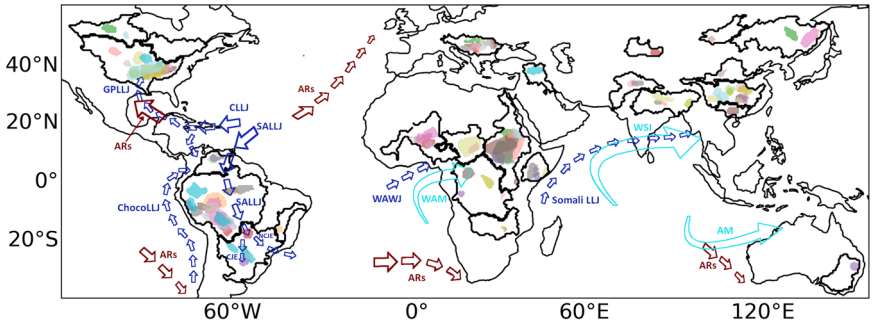

Fig. 1 | Geographical distribution of studied river basins and flood events. Map showing the location of 24 river basins (black contours) affected by 119 flood events, with coloured regions indicating the corresponding flood-affected areas. River basins boundaries from HydroBASINS project at https://www.hydrosheds.org. Arrows represent the major mechanisms of moisture transport at the global scale: Atmospheric Rivers (ARs; dark red arrows), Low-Level Jets (LLJs; blue arrows), and monsoon systems (cyan arrows). The main LLJs are indicated: The Great Plains Low-Level Jet (GPLLJ), the Chocó Low-Level Jet (ChocoLLJ), the South American Low-Level Jet (SALLJ), the Caribbean Low-Level Jet (CLLJ), the West African Westerly Jet (WAWJ), and the Somali Low-Level Jet (Somali LLJ). The two-phase nature of the SALLJ is highlighted, distinguishing between the Chaco Jet Event (CJE) and the No-Chaco Event (NCJE). The major monsoon regimes are also indicated: The West African Monsoon (WAM), Western and Southern India (WSI), and the Australian Monsoon (AM).

Southeast Asia). This limitation reflects the constraints of our basin-focused analytical framework rather than a diminished importance of flooding in these regions, or the potential role of AR-like features within monsoon systems in generating these floods.

When the river basin was considered to be the reference area, ARs coincided with nearly 90% of the flood events during the core flood period and ~30% of all 3 days prior to the events (Fig. 2a). To assess the robustness of these associations across spatial scales, we also analysed hydrobasins sub-basin levels 4 and 5 areas, which represent more hydrologically constrained domains than entire river basins. AR coincidences during flood events decreased systematically to 79% (level 4) and 77% (level 5), demonstrating spatial scale dependence while maintaining high association rates. The coincidences for days −1, −2, and −3 individually were similar, with ARs affecting ~55–57% of the events on each of those days at the river basin scale. At sub-basin scales, individual daily percentages ranged from 34 to 49% (level 4) and 27 to 38% (level 5), with percentages increasing from day −1 to day −3. Collectively, ARs during the three preceding days coincided with 30% (river basin), 29% (level 4), and 24% (level 5) of flood events. When the flood-affected area was used as the reference area, the percentage of flood events in which ARs were present decreased but remained above 70%. In contrast, the coincidence of ARs during the preceding days decreased markedly to about half, and even less when assessed collectively for all 3 days. These findings suggest that ARs frequently precede flood onset and impact broader upstream regions, even without directly overlapping with flooded zones, highlighting the potential key role of the river basin in modulating surface runoff and flood generation.

At the river basin scale, the majority of floods events (60 events), showed AR-related precipitation representing less than 10% (Fig. 2b). Lower distributions in the 0–10% range were observed at sub-basin scales, with 45 and 44 events at levels 4 and 5, respectively, whereas ~40 events fell into this range when the flood area was considered. However, for the remaining precipitation percentage ranges, the number of events across spatial scales does not differ substantially. Notably, more events were recorded in flood-affected areas, where AR-related precipitation accounted for more than 80% of the total precipitation. Overall, these results highlight a potential spatial mismatch between the precipitation footprint of ARs and the actual extent of the resulting floods. This mismatch arises because flood generation depends not only on precipitation location but also on basin-scale hydrological processes, including upstream–downstream water routing, antecedent soil moisture conditions, and drainage network configuration. Statistical analysis confirmed that ~72% of events in which ARs intersected the flood area, and about 67.0% of events with AR presence in the river basin showed precipitation significantly above climatological values ($p < 0.10$). When constrained to sub-basin scales, 72.3% (level 4) and 73.0% (level 5) of events showed significant AR associations, confirming that approximately three-quarters of major floods remain robustly associated with ARs even under spatially refined hydrological assessment.

Next, we analysed the AR-driven precipitation during the 3 days preceding flood onset, determining the number of flood events categorised by the precipitation percentage attributable to ARs across different spatial scales. For most events, AR-associated precipitation accounted for a relatively low percentage of the total rainfall over the entire river basin during each of the 3 days preceding flood onset (Fig. 2c). At sub-basin scales (Fig. 2d, e) days −3 and −2 show the highest number of events in low contribution bins (f_AR < 20%). This pattern reverses dramatically at high contribution bins (f_AR > 70%), where day −1 dominates, particularly at level 5. This pattern aligns with the distribution observed during the flood period itself (Fig. 2f), suggesting that upstream AR-driven precipitation, although not always intense, play a critical role in increasing antecedent soil moisture, as confirmed in Fig. S1, and thus increasing the basin's vulnerability to flooding from subsequent rainfall, as stated in previous findings (e.g. Webb et al.[19]).

In contrast, a considerable number of events fall in the highest precipitation bins (80–90% and 90–100%), particularly on the day immediately preceding flood onset (Fig. 2d–f). This result indicates that, in many cases, nearly all the rainfall triggering the flood originated from a single AR event occurring just 1 day before the flood, supporting the idea that ARs often serve not only as contributing factors but also as the principal hydrometeorological drivers of flood events, which have been demonstrated to affect water availability[9]. Conversely, days −2 and −3 are associated with markedly fewer events associated with higher precipitation, indicating that while ARs may influence atmospheric and soil conditions up to 72 h in advance, their peak hydrological impact is concentrated within the 24 h immediately preceding the flood. This temporal clustering suggests that ARs play dual roles as both immediate flood triggers and antecedent preconditioners that progressively saturate catchments, thereby lowering the threshold for runoff generation and amplifying the flood response when subsequent rainfall occurs, whether from continued AR activity or other weather systems. This preconditioning effect has significant implications for flood forecasting and early warning. In addition, climate warming is expected to intensify water vapour transport in ARs by 6.3–9.7% per degree Celsius of warming[20], altering their frequency, duration, and geographical distribution, implying a significant contribution to future flood risk[21].

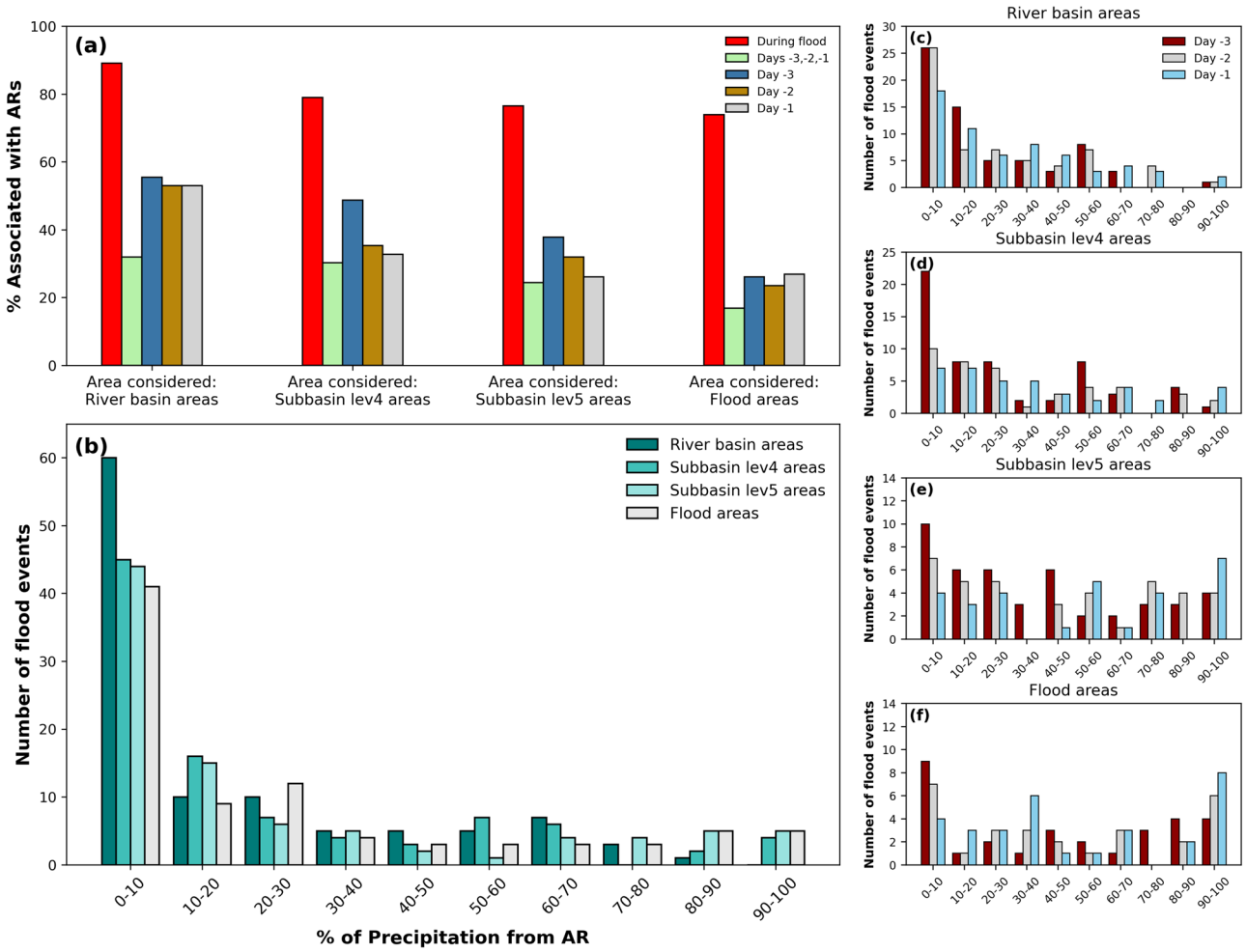

Fig. 2 | Association between atmospheric rivers and flood events. a Percentage of flood events and the three days prior to flood onset coincident with ARs considering either the river basin area, sub-basin level 4, sub-basin level 5, and flood area. **b** Number of flood events with total precipitation percentages attributed to ARs in various ranges over the basin, sub-basin level 4, sub-basin level 5, and flood areas. Number of flood events with total precipitation percentages attributed to ARs for **c** river basin areas, **d** sub-basin level 4 areas, **e** sub-basin level 5 areas, and **f** flood areas.

These results are based on the tARget v4 AR detection algorithm using the 85th percentile threshold of the Integrated Vapour Transport (IVT). Although this threshold is widely accepted and validated across multiple regions, the different detection methods or thresholds could yield different absolute percentages of AR-associated floods. Indeed, the Atmospheric River Tracking Method Intercomparison Project (ARTMIP) has shown that tropical regions exhibit the largest variance in AR frequency among different catalogues, with disagreement concentrated primarily due to high humidity that confounds certain detection methodologies, and different approaches to marginal detections[22]. Consequently, our conclusions remain robust across different methodologies, as they rely on the physical AR-flood association instead of being tied to specific AR intensity thresholds.

To assess the broader societal implications of AR-driven floods, we analysed the human impacts of the 106 AR-associated flood events across affected river basins from 1999 to 2018, examining spatial patterns of inundation, mortality, and population displacement. Indeed, since 2000, flood-related disasters have increased by 134% compared with the previous two decades[23], with ARs contributing substantially to this trend. The spatial analysis reveals that AR-induced floods show annual recurrent impacts and larger inundation areas across tropical and subtropical basins. It is well observed in the Amazon and Mississippi River basins in South and North America, respectively, the basins across the Sahel region in Africa, and the Yangtze River in China (Fig. 3a). The annual total affected area exhibits marked interannual variability, with peak years such as 2004 and 2014 showing the highest cumulative flood extent (Fig. 3b). These findings demonstrate that AR-flood impacts affect regions with high population density and economic activity, where flood-prone river basins coincide with centres of human settlement.

Flood-related mortality displays substantial spatial heterogeneity, with the highest death tolls reported in the Niger River and Nile River basins in Africa and the Yangtze River Basin in China (Fig. 3c). The temporal evolution of this indicator reveals pronounced peaks in 2006, 2012, 2014, and 2016 (Fig. 3d). These areas are highly vulnerable to floods and make up nearly three-quarters of the total modelled displacement, averaging almost 10 million globally each year[24]. The displacement of populations due to AR-associated floods during the study period was most pronounced in the Nile River basin, the Andean region southwest of the Amazon River basin, and the southeast of the Mississippi River Basin (Fig. 3e). The temporal profile of displaced persons reveals a notable maximum in 1999, followed by a secondary peak in 2006, which is consistent with years of elevated mortality (Fig. 3f).

This study reveals that ARs function as a near-universal driver of major flood events in river basins across diverse climate zones and hydrological regimes. However, further research is needed to develop improved methods for quantifying how antecedent AR-related precipitation drives flooding preconditions in catchments, for example, the land use changes, or infrastructure modifications that influence flood generation. These limitations do not fundamentally undermine our core findings, as a large sample size

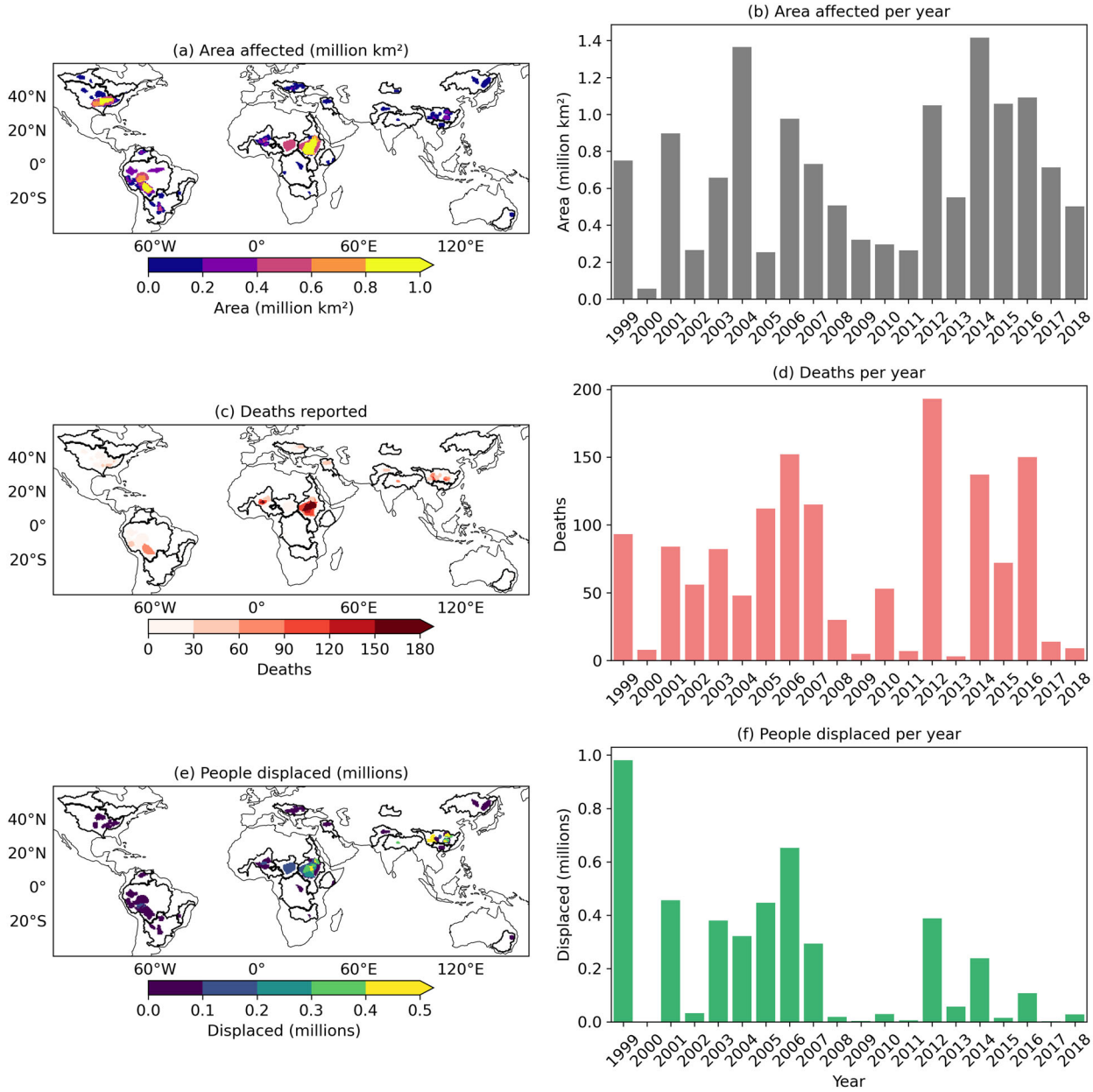

Fig. 3 | Global distribution and impacts of floods during 1999–2018. a Locations of floods with colour scale representing the total geographical area affected (million km²). **b** Annual total area affected by floods. **c** Reported deaths and their locations. **d** Annual total deaths. **e** People displaced due to floods and their corresponding locations (millions). **f** Annual total displaced population.

and robust statistical associations provide strong evidence. In addition, the potential for using AR characteristics (intensity, duration, orientation) as predictors of flood magnitude and extent, beyond simple precipitation forecasts, should be explored. This would enable more targeted adaptation strategies in future AR scenarios, to avoid major impacts on society, agriculture and finally the economy.

Methods

Flood event database

The flood event records were obtained from the DFO[17], which is accessible at https://floodobservatory.colorado.edu. This database was used to identify flood occurrences across 50 representative river basins worldwide, covering a broad range of climatic regions, hydrological regimes, and socio-environmental contexts (Table S2) over 20 years (1999–2018), which we set as the study period. The information compiled in this archive is derived from a combination of sources, including news reports, governmental records, instrumental measurements, and satellite-based remote sensing. The archive provides detailed records of flood events, encompassing key attributes that were used in this study, such as spatial outlines of affected areas, onset and end dates, event durations, and associated impacts, including reported fatalities and numbers of displaced persons.

Atmospheric river detection

The global atmospheric river database developed by Guang and Waliser[25] was also utilised. These authors implemented the tARget v4.0 (Tracking Atmospheric Rivers Globally as Elongated Targets) algorithm to provide daily, objectively detected AR footprints based on the IVT magnitude (areas exceeding the 85th percentile threshold) and direction derived from ERA5

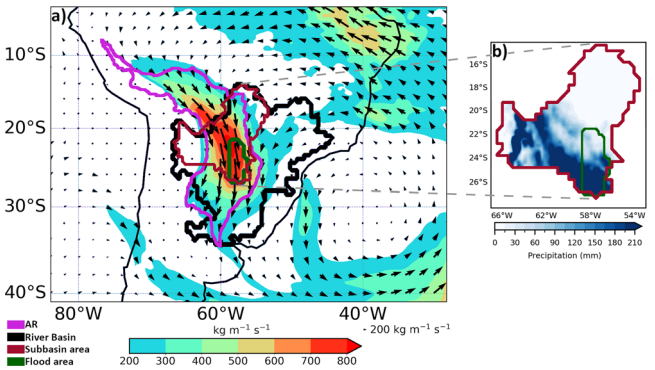

Fig. 4 | Example of coincidence between an atmospheric river and a flood-affected area. a The La Plata River basin (black contour) and the flood-affected area (blue contour) during 4–15 July 2013 are shown together with the footprint of an atmospheric river (magenta contour). Coloured shading depicts the vertically integrated water vapour transport (IVT, kg m^{-1} s^{-1}), and arrows indicate the direction and magnitude of the moisture flux. **b** Accumulated precipitation during 4–15 July 2013 in the selected sub-basin.

reanalysis at 6 h intervals and a 0.25° × 0.25° horizontal resolution. An object is retained if its length exceeds 2000 km and has a length-to-width ratio greater than 2. This criterion ensures that only long and narrow objects, characteristic of ARs, are kept. They also implemented an algorithm to better handle ARs in tropical and polar areas and zonal ARs, which is crucial to identify AR-like structures in tropical regions where the background moisture content is naturally relatively high and where traditional fixed-threshold approaches might miss AR events. Thus, the term AR in this study refers to structures objectively detected by this algorithm, which in tropical regions may differ dynamically (e.g. monsoon moisture surges, tropical plumes, cross-equatorial flows) from classical extratropical ARs. However, these features share the fundamental characteristic of transporting anomalously high amounts of water vapour in coherent, elongated structures that justify the use of a unified detection framework[4].

Flood selection criteria

From the DFO archive, we selected flood events that (1) occurred within any of the 50 pre-selected river basins and (2) had their entire flood-affected area completely contained within a single basin boundary. This spatial containment criterion ensured unambiguous AR-flood attribution and avoided complications from floods spanning multiple basins or extending beyond basin limits. Given the very large spatial extent of some of the major river basins considered, flood attribution was further refined by identifying the HydroBASINS sub-basins (levels 4 and 5) intersecting each flood-affected area. These sub-basins represent hierarchically nested subdivisions of the original basins that preserve upstream–downstream connectivity, allowing the spatial extent of each flood event to be characterised within smaller, hydrologically coherent units.

Attribution of precipitation to ARs

To quantify the fraction of precipitation attributable to ARs, we used daily precipitation data from the Multi-Source Weighted-Ensemble Precipitation (MSWEP) dataset version 2.8 at 0.1° spatial resolution[26]. For each flood event, we identified the spatial overlap between the AR footprint from the tARget database and the flood-affected area from DFO for each day during the flood period and the three preceding days. We then calculated the total precipitation over the entire flood-affected area (P_total) and the precipitation within the AR-flood intersection area (P_AR). The fraction of precipitation attributable to the AR was computed as f_AR = (P_AR / P_total) × 100, representing the percentage of total flood-area precipitation that occurred within pixels where an AR was present. This fraction was calculated separately for each flood event and for each of the 3 days preceding the flood onset, which allow to assess both immediate triggers and antecedent conditioning effects. When the AR footprint completely covered the flood-affected area, f_AR = 100%, indicating all precipitation was AR-related, whereas f_AR = 0% when no AR was present over the flood area. This analysis was conducted at multiple spatial supports, including the flood-affected area, the intersecting HydroBASINS level 4 and 5 sub-basins, and the corresponding major river basin, in order to assess the sensitivity of AR–precipitation attribution to spatial aggregation and to better approximate hydrological connectivity.

As an example, representative for all cases, we present the spatial extent of a flood event (blue line) that affected the La Plata River basin from 4 to 15 July 2013 (Fig. 4). The shape of the AR is delineated by the magenta line, covering the whole flood area and intersecting part of the river basin. In this case, we considered this AR to be associated with the flood area and the river basin. The vectors show the IVT arriving at the flood area from the northeast, with the maximum values coinciding with the flood area, and the rainfall observed over subbasin 4, primarily in the southern half. This approach provides a consistent and objective metric for assessing AR contributions across our global dataset, under the assumption that precipitation falling within the AR footprint can be attributed to AR-related moisture transport.

Assessment of precipitation anomalies

To assess whether the accumulated precipitation during each event was anomalous with respect to the long-term climatology, we first calculated the total precipitation of the event over its duration in the year of occurrence. For comparison, we then computed the accumulated totals for the same calendar days in all other years of the record, thereby constructing a reference distribution. Statistical significance was evaluated by contrasting the event total against the distribution mean, while accounting for temporal autocorrelation through an effective sample size adjustment. A confidence level of 0.90 was adopted to identify those events with total precipitation considered statistically significant.

Data availability

The AR database used in this study is publicly available at https://doi.org/10.6084/m9.figshare.c.6953288.v1. The flood inventory data are available at [https://floodobservatory.colorado.edu]. The daily MSWEP reanalysis data are available at https://www.gloh2o.org/mswep/. The GLEAM data are available at [https://www.gleam.eu/]. The Python scripts used for processing the data are available from the corresponding author upon reasonable request.

Received: 5 September 2025; Accepted: 9 January 2026;
Published online: 15 January 2026

References

1. Zhu, Y. & Newell, R. E. A proposed algorithm for moisture fluxes from atmospheric rivers. *Mon. Weather Rev.* **126**, 725–735 (1998).
2. Ralph, F. M., Dettinger, M. D., Cairns, M. M., Galarneau, T. J. & Eylander, J. Defining "atmospheric river": how the glossary of meteorology helped resolve a debate. *Bull. Am. Meteor. Soc.* **99**, 837–839 (2018).
3. *AMS (American Meteorological Society), 2017: Atmospheric River*. Glossary of Meteorology. http://glossary.ametsoc.org/wiki/Atmospheric_river.
4. Gimeno, L., Algarra, I., Eiras-Barca, J., Ramos, A. M. & Nieto, R. Atmospheric river, a term encompassing different meteorological patterns. *Wiley Interdiscip. Rev. Water* **8**, e1558 (2021).
5. Reid, K. J., King, A. D., Lane, T. P. & Hudson, D. Tropical, subtropical, and extratropical atmospheric rivers in the Australian region. *J. Climate* **35**, 2697–2708 (2022).
6. Waliser, D. & Guan, B. Extreme winds and precipitation during landfall of atmospheric rivers. *Nat. Geosci.* **10**, 179–183 (2017).
7. Wang, W. et al. Local floods induce large-scale abrupt failures of road networks. *Nat. Commun.* **10**, 2114 (2019).

8. Ionita, M., Nagavciuc, V. & Guan, B. Rivers in the sky, flooding on the ground: the role of atmospheric rivers in inland flooding in central Europe. *Hydrol. Earth Syst. Sci.* **24**, 5125–5147 (2020).
9. Paltan, H. et al. Global floods and water availability driven by atmospheric rivers. *Geophys. Res. Lett.* **44**, 10,387–10,395 (2017).
10. Dettinger, M. D. Atmospheric rivers as drought busters on the U.S. West Coast. *J. Hydrometeor.* **14**, 1721–1732 (2013).
11. Liu, Q. et al. Global, regional and national trends and impacts of natural floods, 1990–2022. *Bull. World Health Organ.* **102**, 410–420 (2024).
12. Intergovernmental Panel on Climate Change (IPCC). *Water Cycle Changes. In Climate Change 2021 – The Physical Science Basis: Working Group I Contribution to the Sixth Assessment Report of the Intergovernmental Panel on Climate Change*. 1055–1210 (Cambridge Univ. Press, 2023).
13. Swain, D. L. et al. Increased flood exposure due to climate change and population growth in the United States. *Earth's Future* **8**, e2020EF001778 (2020).
14. Tabari, H. Climate change impact on flood and extreme precipitation increases with water availability. *Sci. Rep.* **10**, 13768 (2020).
15. Lavers, D. A. & Villarini, G. The contribution of atmospheric rivers to precipitation in Europe and the United States. *J. Hydrol.* **522**, 382–390 (2015).
16. Zhou, Y. et al. Atmospheric river frequency-category characteristics shape U.S. West Coast runoff. *J. Geophys. Res. Atmos.* **130**, e2024JD041805 (2025).
17. Lehner, B. & Grill, G. Global river hydrography and network routing: baseline data and new approaches to study the world's large river systems. *Hydrol. Processes* **27**, 2171–2186 (2013).
18. Brakenridge, G. R. *Global Active Archive of Large Flood Events. DFO - Flood Observatory* (University of Colorado, USA, accessed 24 June 2025) http://floodobservatory.colorado.edu/Archives/.
19. Webb, M. J., Albano, C. M., Harpold, A. A., Wagner, D. M. & Wilson, A. M. Wet antecedent soil moisture increases atmospheric river streamflow magnitudes nonlinearly. *J. Hydrometeor.* **26**, 741–758 (2025).
20. McClenny, E. E., Ullrich, P. A. & Grotjahn, R. Sensitivity of atmospheric river vapor transport and precipitation to uniform sea surface temperature increases. *J. Geophys. Res. Atmos.* **125**, e2020JD033421 (2020).
21. Payne, A. E. et al. Responses and impacts of atmospheric rivers to climate change. *Nat. Rev. Earth Environ.* **1**, 143–157 (2020).
22. Rutz, J. J. et al. The atmospheric river tracking method intercomparison project (ARTMIP): quantifying uncertainties in atmospheric river climatology. *J. Geophys. Res. Atmos.* **124**, 13777–13802 (2019).
23. United Nations Office for Disaster Risk Reduction (UNDRR). *Global Assessment Report on Disaster Risk Reduction 2025: Resilience Pays – Financing and Investing for Our Future*. (UNDRR, Geneva, 2025).
24. Internal Displacement Monitoring Centre (IDMC). *Systematic Data Collection and Monitoring of Displacement and Its Impacts at Local, National, Regional and International Level to Inform Comprehensive Needs and Risk Assessments for the Formulation of Policy and Plans (WIM Task Force on Displacement Activity III.1-3 Output)* (IDMC, 2018). https://unfccc.int/sites/default/files/resource/WIM%20TFD%20III.1-3%20Output.pdf.
25. Guan, B. & Waliser, D. E. A regionally refined quarter-degree global atmospheric rivers database based on ERA5. *Sci. Data* **11**, 440 (2024).
26. Beck, H. E. et al. MSWEP V2 global 3-hourly 0.1° precipitation: methodology and quantitative assessment. *Bull. Am. Meteorol. Soc.* **100**, 473–500 (2019).

Acknowledgements

M.S. and A.P-A. are thankful for the support from Xunta de Galicia (Consellería de Cultura, Educación, Formación Profesional e Universidades) under Postdoctoral Grant Nos. ED481D−2024/017 and ED481B−2023/016, respectively. R.S. acknowledges grant RYC2021−034044-I funded by the Ministerio de Ciencia, Innovación y Universidades, Spain (MICIU/AEI/https://doi.org/10.13039/501100011033) and the European Union Next Generation EU/PRTR. A.P-A., M.S. and R.S. are also supported by the project Excelencia-ED431F-2024/03 funded by the Xunta de Galicia. EPhysLab members are supported by the SETESTRELO project (grant no. PID2021−122314OB-I00) funded by the Ministerio de Ciencia, Innovación y Universidades, Spain (MICIU/AEI/https://doi.org/10.13039/501100011033), Xunta de Galicia under the Project ED431C2021/44 (Programa de Consolidación e Estructuración de Unidades de Investigación Competitivas (Grupos de Referencia Competitiva) and Consellería de Cultura, Educación e Universidade). This work was also made possible by the computing resources and technical support provided by Climate System Research Unit, UVigo-CESGA.

Author contributions

Conceptualization: M.S., A.P.-A., R.S, R.N., L.G. Methodology: M.S., R.S, L.G. Investigation: M.S., A.P.-A., R.S. Software: M.S., A.P.-A., R.S. Data Curation: M.S., A.P.-A., R.S. Visualization: M.S., R.S. Supervision: R.N., L.G. Writing—original draft: M.S., R.S. Writing – review and editing: M.S., A.P.-A., R.S, R.N., L.G.

Competing interests

The authors declare no competing interests.

Additional information

Supplementary information The online version contains supplementary material available at https://doi.org/10.1038/s44304-026-00167-x.

Correspondence and requests for materials should be addressed to Milica Stojanovic.